00

Alternative phase functions in the modelling of coherent backscattering

© V.L. Kuzmin[1], Yu.A. Zhavoronkov[1,2], S.V. Ul'yanov[2]

[1]Peter the Great Saint-Petersburg Polytechnic University,
195251 St. Petersburg, Russia
[2]St. Petersburg State University,
199034 St. Petersburg, Russia

e-mail: kuzmin_vl@mail.ru

Received July 26, 2023
Revised April 06, 2024
Accepted April 06, 2024

Modelling of the coherent backscattering effect based on the Bethe–Solpeter equation has been carried out when anisotropy is taken into account using two different phase functions. It is found that with increasing anisotropy of the single scattering indicatrix, calculations with the Rayleigh–Gans phase function lead to wider angular peaks of coherent backscattering than calculations with the Henya–Greenstein phase function. Monte Carlo simulations of coherent backscattering based on the Rayleigh–Hans phase function have been performed for the first time. On the basis of alternative phase functions, the effect of decreasing the spatial coherence length of the incident radiation on the shape of the angular peak of coherent backscattering is investigated. It is shown that with decreasing coherence length both models lead to broadening of the peak, which can be used in biomedical diagnostics.

Keywords: Coherent backscattering, Monte Carlo simulations, Bethe–Solpeter equation.

DOI: 10.61011/EOS.2024.04.58883.5453-24

1. Introduction

Optical methods of medical diagnostics have progressed rapidly in the last decade [1–6]. The so-called „transparency window" in the near infrared region makes it possible to retrieve data from radiation scattered by the biological environment, and the actual harmlessness of this radiation enables its use in the study of living organisms. The discovery of coherent [7–14] and correlation [15,16] effects in multiple scattering in randomly inhomogeneous media led to the development of near infrared spectroscopy (NIRS) and diffuse correlation spectroscopy (DCS) in application to biological systems. Different types of infrared radiation are used in experiments: continuous-wave (CW) irradiation of biological tissues [17–20], short pulses [21–24], or radiation with various types of modulation [21,25,26]. In the present study, we examine the scattering of a continuous plane laser wave incident on a flat boundary of a semi-infinite randomly inhomogeneous medium. Particular attention is paid to the effect of coherent backscattering (CBS) enhancement in which the wave nature of multiply scattered radiation is manifested most clearly. Note that the extreme narrowness of the CBS cone angle [12–14] is a significant hindrance to the application of CBS in biomedical practice. Therefore, one of the important tasks is the preparation and modeling of systems and settings in which the CBS cone angle gets wider.

When one determines the physiological state of biological tissues based on scattered radiation data, it is important to know the optical parameters of a random medium: scattering coefficient μ_s and absorption coefficient μ_a. It is crucial to take into account the anisotropy of the single scattering indicatrix or the phase function when these coefficients are being established. The experimentally determined value is reduced scattering coefficient μ'_s, which is related to scattering coefficient μ_s as $\mu'_s = (1-g)\mu_s$ [27], where parameter $g = \langle \cos\theta \rangle$ is the average cosine of the single scattering angle. Thus, parameter g in the lowest-order approximation does already characterize the anisotropy of the phase function; at the same time, all kinds of phase functions characterizing the anisotropy of single scattering may yield the same value of $\langle \cos\theta \rangle$. Therefore, the problem of comparing the results of backscattering calculated with different model phase functions arises naturally in multiple scattering. The empirical Henyey–Greenstein (HG) phase function, which includes parameter g directly, is the one used most often to model anisotropic scattering. The popularity of this phase function rests mainly on its mathematical convenience. Disadvantages of the HG model include the lack of its justification at the „micro level"; this phase function is not a calculated indicatrix of scattering by a certain type of inhomogeneity in biological tissue. The scattering anisotropy and parameter g itself depend on the physical properties of scatterers and, most notably, on their sizes. The simplest model taking into account the type of scattering particles and their sizes is the model of a suspension of hard spheres, which corresponds, e.g., to red blood cells. In the lowest-order approximation in permittivity deviations, this model gives rise to the Rayleigh–Gans (RG) phase function. The present study is focused on numerical modeling with these two phase functions (HG and RG). The description of scattering based on Mie formulae is formally more accurate than the RG model, but it is rather difficult in a mathematical sense to

use Mie formulae in modeling. Note that the degree of anisotropy of single scattering in the RG and Mie models is specified by dimensionless parameter kR, where R is the particle radius and k is the wave number.

In the present study, the intensity of laser radiation backscattered by a biological medium was calculated on the basis of the Bethe–Salpeter equation, which was used to characterize the transfer of radiation in a randomly inhomogeneous medium. The iterative solution of this equation yields the scattered intensity presented as a series in scattering multiplicities. The terms of this series are multiple integrals that were calculated using the Monte Carlo (MC) method. The modeling method developed here allowed us to determine the degree of influence of the anisotropy type of the single scattering indicatrix on the calculation results. The results obtained using the HG and RG indicatrices were compared for this purpose. A comparative analysis of the results of calculations of the backscattering intensity as a function of the distance between a source and a detector located on the surface of a semi-infinite randomly inhomogeneous medium has been performed earlier in [28] for the HG and RG phase functions. Calculations were carried out within a wide angular range with account only for the primary (incoherent) contribution to the scattering intensity, which corresponds to the use of the Bethe–Salpeter equation in the ladder approximation. Since the present report is focused on the CBS peak region, coherent and incoherent contributions to scattering were taken into account in calculations with the HG and RG model functions. The inverse transform method [29], which consists in inverting the integral (cumulative) distribution function of random spatial variables (scattering angles and free path length), was used in our implementation of the MC algorithm. The inverse transform of the cumulative distribution function is easy to perform for the model HG indicatrix, and the result is presented as an elementary function. In the present work, an explicit form of the cumulative distribution function found for the RG model allowed us to implement efficiently the inverse transform method for this model and, in a scientific first, simulate multiple scattering for both types of phase functions simultaneously.

Broadening of the CBS cone with a reduction in the degree of spatial coherence of incident radiation is another important CBS effect. When modeling the reduction in spatial coherence, we vary the number of scattering multiplicities taken into account. The obtained calculated data revealed that the use of low-coherence radiation allows one to obtain a CBS cone with width and relative height values close to the experimental ones [12].

2. Radiation transfer

The transfer of steady-state radiation in an infinite randomly inhomogeneous medium may be characterized by the Bethe–Salpeter equation

$$\Gamma(\mathbf{r}_2, \mathbf{r}_1|\,\mathbf{k}_s, \mathbf{k}_i) = \frac{k_0^4}{4\pi^2} G(\mathbf{k}_s - \mathbf{k}_i)\delta(\mathbf{r}_2 - \mathbf{r}_1)$$
$$+ \frac{k_0^4}{4\pi^2} \int d\mathbf{r}_3 G(\mathbf{k}_s - \mathbf{k}_{23})\Lambda(\mathbf{r}_2 - \mathbf{r}_3)\Gamma(\mathbf{r}_3, \mathbf{r}_1|\mathbf{k}_{23}, \mathbf{k}_i), \quad (1)$$

where coherence function $\Gamma(\mathbf{r}_2, \mathbf{r}_1|\mathbf{k}_s, \mathbf{k}_i)$ characterizes the propagation of radiation incident at point $\mathbf{r}_1$ and emerging at $\mathbf{r}_2$ with initial and final wave vectors $\mathbf{k}_i$ and $\mathbf{k}_s$, respectively; $\mathbf{k}_{ij} = k_0\mathbf{r}_{ij}/r_{ij}$; $\mathbf{r}_{ij} = \mathbf{r}_i - \mathbf{r}_j$; $k_0 = 2\pi/\lambda$ is the wave number; and λ is the wavelength in vacuum. The product of two complex–conjugate average Green's functions of a scalar field yields single scattering propagator $\Lambda(r) = r^{-2}\exp(-\mu r)$, where $\mu = \mu_s + \mu_a$ is the extinction coefficient. $G(\mathbf{k})$ is the Fourier transform of the correlation function of permittivity fluctuations:

$$G(\mathbf{k}) = \int d(\mathbf{r} - \mathbf{r}_0)e^{-i\mathbf{k}\cdot(\mathbf{r}-\mathbf{r}_0)}\langle\delta\varepsilon(\mathbf{r})\delta\varepsilon^*(\mathbf{r}_0)\rangle.$$

The optical theorem relates scattering coefficient μ_s to the integrated intensity of single scattering, and both these quantities are expressed through correlation function $G(\mathbf{k})$; in the case of a scalar field,

$$\mu_s = \frac{k_0^4}{(4\pi)^2} \int d\Omega_s G(\mathbf{k}_s - \mathbf{k}_i). \quad (2)$$

The Rayleigh factor is added to (2) for an electromagnetic field: $G \to G(1 + \cos^2\theta_s)/2$.

Having introduced the normalized phase function

$$p(\hat{\mathbf{k}}_s\hat{\mathbf{k}}_i) = G(\mathbf{k}_s - \mathbf{k}_i)/\int d\Omega_s G(\mathbf{k}_s - \mathbf{k}_i),$$

where $\hat{\mathbf{k}}$ denotes a unit vector along $\mathbf{k}$, one may rewrite Eq. (1) in the following form:

$$\Gamma(\mathbf{r}_2, \mathbf{r}_1|\mathbf{k}_s, \mathbf{k}_i) = \mu_s p(\hat{\mathbf{k}}_s\hat{\mathbf{k}}_i)\delta(\mathbf{r}_2 - \mathbf{r}_1)$$
$$+ \mu_s \int d\mathbf{r}_3 p(\hat{\mathbf{k}}_s\hat{\mathbf{k}}_{23})\Lambda(\mathbf{r}_2 - \mathbf{r}_3)\Gamma(\mathbf{r}_3, \mathbf{r}_1|\mathbf{k}_{23}, \mathbf{k}_i). \quad (3)$$

Note that the phase function depends only on the cosine of angle θ between the vectors that are its arguments; i.e., $p(\hat{\mathbf{k}}_s, \hat{\mathbf{k}}_i) = p(\cos\theta)$.

3. MC modeling

Let z be the Cartesian coordinate of point $\mathbf{r} = (\mathbf{r}_\perp, z)$ normal to the boundaries of a plane-parallel layer with thickness T ($0 \le z \le T$, including the case of a semi-infinite medium, $z \ge 0$). Within a constant dimensional factor, the main incoherent part of intensity of radiation scattered into the upper half-space („backscattered" radiation)

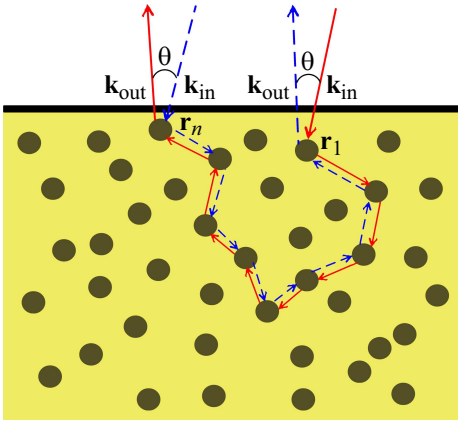

Figure 1. Schematic representation of the coherence effect in backscattering. Phase differences between the field and its complex conjugate, which propagated in the opposite direction, are preserved in backscattering.

is [28,29,30]

$$J(\mathbf{k}_i, \mathbf{k}_s) = 4\pi \int_0^\infty dz_1 \int_{z_2>0} d\mathbf{r}_2 \Gamma(\mathbf{r}_2, \mathbf{r}_1 | \mathbf{k}_s, \mathbf{k}_i) \times \exp\left(-\mu\left(\frac{z_2}{\cos\theta_s} + \frac{z_1}{\cos\theta_i}\right)\right),$$

where θ_i is the incidence angle and θ_s is the backscattering angle measured from the direction opposite to axis z. The iterative solution of Bethe–Salpeter equation (3) yields a representation of intensity in the form of a series in scattering multiplicities:

$$J(\mathbf{k}_i, \mathbf{k}_s) = \sum_{n=1}^{\infty} J^{(n)}(\mathbf{k}_i, \mathbf{k}_s), \qquad (4)$$

where $J^{(n)}(\mathbf{k}_i, \mathbf{k}_s)$ is the contribution of the nth scattering order.

Within the ladder approximation based on the Bethe–Salpeter equation, we present term $J^{(n)}(\mathbf{k}_i, \mathbf{k}_s)$ of order n as the average over a sample of N_{ph} incident photons:

$$J^{(n)}(\mathbf{k}_i, \mathbf{k}_s) = \frac{1}{N_{\text{ph}}} \sum_{j=1}^{N_{\text{ph}}} W_n^{(j)}(\mathbf{k}_i, \mathbf{k}_s) \times p\left(\hat{\mathbf{k}}_{n\,n-1}^{(j)} \hat{\mathbf{k}}_s\right) f_{\text{BLB}}(\mathbf{k}_i, \mathbf{k}_s, z_1^{(j)}, z_n^{(j)}), \qquad (5)$$

where $W_n^{(j)}(\mathbf{k}_i, \mathbf{k}_s)$ and $z_n^{(j)}$ are the weight and the distance from the boundary to point $\mathbf{r}_n^{(j)}$ of the nth scattering event, respectively. Bouguer–Lambert–Beer factor $f_{\text{BLB}}(\mathbf{k}_i, \mathbf{k}_s, z_1^{(j)}, z_n^{(j)})$ characterizes the propagation of radiation from the entry point to the point of first scattering and, in the Fraunhofer approximation, from the point of nth scattering to its emergence from the medium. It depends on the optical parameters of the medium in the photon path and on the photon flux geometry. When scattering in the CBS region is studied, one needs to introduce into sum (4) the contributions not only of ladder diagrams, but also of maximally crossed diagrams [20].

Weight $W_n^{(j)}$ is a random value of a multiple spatial integral emerging as the nth order iteration of the Bethe–Salpeter equation. Calculating it, one may model a stochastic sequence (or trajectory) of scattering points $\mathbf{r}_1, \ldots \mathbf{r}_n$. The complete sum of ladder diagrams, which is practically independent of the backscattering angle in the region of the backscattering peak, is denoted as $J_L(\mathbf{k}_i, \mathbf{k}_s) = \sum_n J_L^{(n)}(\mathbf{k}_i, \mathbf{k}_s)$, and the complete sum of maximally crossed diagrams is

$$J_C(\mathbf{k}_i, \mathbf{k}_s) = \sum_n J_C^{(n)}(\mathbf{k}_i, \mathbf{k}_s).$$

For a wave backscattered at angle $\theta = \theta_s$ (see Fig. 1), function $f_{\text{BLB}} = F_L$ in expression (5) in the terms with ladder contributions. where

$$F_L\left(\mathbf{r}_1^{(j)}, \mathbf{r}_n^{(j)}\right) = \exp\left(-\mu(z_1^{(j)} + z_n^{(j)}/\cos\theta_s)\right),$$

while $f_{\text{BLB}} = F_C$ in the terms with contributions from maximally crossed diagrams, where

$$F_C\left(\mathbf{r}_1^{(j)}, \mathbf{r}_n^{(j)}\right) = \exp\left(-\frac{\mu}{2}\left(z_1^{(j)} + z_n^{(j)}\right)\left(1 + \frac{1}{\cos\theta_s}\right)\right) \times \exp\left[ik\left(x_1^{(j)} - x_n^{(j)}\right)\sin\theta_s + ik\left(z_1^{(j)} - z_n^{(j)}\right)(1 - \cos\theta_s)\right].$$

The MC method in radiation transfer theory is based on the well-known inverse transform procedure [29,32,33], which allows one to transform an integral with an exponential distribution over semi-infinite interval $[0, \infty]$ into an integral with respect to a random variable distributed uniformly over unit interval $[0, 1]$. Within the standard algorithm, the exponent in propagator $\Lambda(r)$ gives the probability density of distribution $f(r) = \mu_s^{-1}\exp(-\mu_s r)$ of random variable r, which is the distance between two successive scattering points for a photon. The integral exponential distribution function is easy to find:

$$\xi = F(r) = 1 - \exp(-\mu_s r),$$

where ξ or $\xi' = 1 - \xi$ are random variables distributed uniformly over unit interval $[0, 1]$. The inverse transform yields

$$r = -\mu_s^{-1} \ln \xi'.$$

The inverse transform method is applied similarly to integrals with respect to angular variables. First, we switch from random scattering angle θ in a scattering event to $t = \cos\theta$, which is then considered as a random variable

distributed in accordance with a given phase function $p(t)$. As was done for spatial variable r, we switch from the integral with respect to variable t to the integral with respect to random variable χ, having defined the integral distribution function

$$\chi = F(t) = 2\pi \int_{-1}^{t} p(t')dt'.$$

Inverse transform $t = F^{-1}(\chi)$ for random variable χ distributed uniformly over unit interval $[0, 1]$ yields random variable t distributed in accordance with phase function $p(t)$. In biomedical applications, the HG phase function is used most often, since it has an important advantage: the inverse transform of cumulative function (6) is performed analytically in explicit form. When the RG phase function is used to characterize single scattering, one gets a chance to model the optical properties of biological tissue based on a physical suspension model, but this approach leads to significant mathematical complications [28,34].

4. Specifics of the inverse transform for the RG phase function

Calculating the scattering intensity in accordance with formula (4), we switch from 3D integration with respect to $\mathbf{r}_j$ to integration with respect to difference variable $\mathbf{r}'_j = \mathbf{r}_j - \mathbf{r}_{j-1}$ for each $j = 2, 3, \ldots$ in succession and find

$$\int d\mathbf{r}'_j \Lambda(r'_j) p(t_j) f(r'_j, t_j) = \frac{1}{2\pi\mu} \times \int_0^1 d\xi_j \int_0^1 d\chi_j \int_0^{2\pi} d\phi_j f\left(-\frac{\ln \xi_j}{\mu}, t(\chi_j)\right), \quad (7)$$

where $f(r'_j, t_j)$ is an arbitrary function, $t_j = t(\chi_j)$ is the function inverse to $\chi_j = \chi(t_j)$ in (6), and ϕ_j is the azimuthal angle. As was noted in Section 3, integration in (7) is performed by averaging over a sample of uniformly distributed random variables $\xi_j, \chi_j \in [0; 1]$ and $\phi_j \in [0; 2\pi]$.

It is known that the RG indicatrix anisotropy is determined entirely by dimensionless parameter kR. Introducing new variable $q = kR\sqrt{2(1-t)}$, which is the modulus of the dimensionless vector of scattering at a particle with radius R, into phase function $p(t)$, we obtain complex function

$$p(t(q)) = p\left(1 - \frac{q^2}{2k^2R^2}\right).$$

In what follows, we write $p(q)$ instead of $p(t(q))$ for simplicity. In these new variables, formula (6) takes the form

$$1 - \chi = 2\pi(kR)^{-2} \int_0^q p(q')q'dq'. \quad (8)$$

The following normalization condition was taken into account here:

$$2\pi(kR)^{-2} \int_0^{2kR} p(q)qdq = 1. \quad (9)$$

If we consider function $2\pi(kR)^{-2}p(q)q$ to be the probability density function of random variable $q \in [0, 2kR]$, function $\chi'(q) = 1 - \chi(q)$, according to (8), is the integral distribution function: the probability that quantity q' assumes a value from the $q' < q$ interval.

The RG phase function [28,35] may be written as

$$p(q) = 2(\pi A)^{-1} q^{-6} (\sin q - q\cos q)^2.$$

Constant $A = (kR)^{-2}F(2kR)$ is determined from normalization condition (9), where function $F(q)$ is given by

$$F(q) = 4 \int_0^q q'^{-5} (\sin q' - q'\cos q')^2 dq'.$$

Importantly, the $F(q)$ function turns out to be elementary:

$$F(q) = q^{-4}(q^4 - q^2 + q\sin 2q - \sin^2 q),$$
$$0 \le F(q) < 1. \quad (10)$$

Thus, normalized quantity $F(q)/F(2kR)$ is actually the integral distribution function of random variable q and may be identified with random variable χ' distributed uniformly over interval $[0, 1]$ in the stochastic inverse transform method:

$$\chi' = F(q)/F(2kR).$$

Note that $q_{\max} = 2kR$. The inverse transform yields q,

$$q = F^{-1}(x), \quad (11)$$

where $x = F(2kR)\chi'$, $0 \le x \le F(2kR) < 1$.

Applying the Lagrange theorem on inversion of series from (10), we obtain expansion

$$q^2 = \frac{9}{2}x\left(1 + \frac{9}{20}x + \frac{81}{280}x^2 + \frac{2403}{11200}x^3 + \ldots\right), \quad (12)$$

which allows for easy determination of inverse function (11). However, series (12) converges only at $|x| < x_1 \approx 0.9528$. The value of $x_1 = F(q_1)$, where $q_1 \approx 4.4934$ is the smallest positive root of transcendental equation

$$\mathrm{tg}(q) = q. \quad (13)$$

The series diverges at point $|x| = x_1$, since $(F^{-1})'(x_1) = \infty$ due to $F'(q_1) = 0$; therefore, expansion (12) may be used in numerical calculations only at x being significantly lower than x_1.

The scattering indicatrix is proportional to $F'(q) = 4(q\cos q - \sin q)^2/q^5$ and turns to zero at points q_n where condition (13) is satisfied,

$$q_n = r_n - r_n^{-1} - \frac{2}{3}r_n^{-3} - \frac{13}{15}r_n^{-5} - \frac{146}{105}r_n^{-7} + \cdots,$$

$r_n = \pi(n + 1/2)$, $n \geq 1$. With a high degree of accuracy, $q_n = (n + 1/2)\pi - ((n + 1/2)\pi)^{-1}$.

The numerical values of sequences q_n and χ_n' make it possible to use model polynomial approximations with a given accuracy. Inverse function $F^{-1}(x)$ has derivative singularities at points $x_n = F(q_n)$: $\left(F^{-1}(x)\right)' \propto (x - x_n)^{-2/3}$. In the numerical algorithm for $F^{-1}(x)$, we use a piecewise smooth approximation such that the function itself is continuous everywhere and its first derivative has correct singularities at all points x_n. A high-order approximation of type (12) is used at small x lying far from $x_1 \approx 0.95$.

5. Results of CBS modeling with the use of two different indicatrices

A small peak width is the main obstacle to application of the CBS enhancement effect in biomedical practice. It has been demonstrated in [36,37] that the peak width increases significantly (while the peak height decreases) with a reduction in the spatial coherence of incident radiation. A reduction in spatial coherence is modeled in the considered computational scheme by lowering the maximum number of scattering events n_{sc}. The following relation between parameter g, which governs the scattering anisotropy in the HG model, and the value of kR in the RG model [28,34] allows one to compare angular dependences of the CBS intensity calculated using the HG and RG indicatrices, the angular distributions of which were presented in [28]:

$$g = \frac{4 - (kR)^{-2}\mathrm{Cin}(4kR)}{F(2kR)} - 3,$$

where $\mathrm{Cin}(x)$ is the integral cosine.

The following matching rules are valid for an incident beam with wavelength $\lambda = 685\,\mathrm{nm}$ in a medium with refraction index $n = 1.33$: $g = 0.773$ for spherical particles with $R = 250\,\mathrm{nm}$ and $g = 0.925$ for $R = 500\,\mathrm{nm}$. The indicatrix is isotropic if $g = 0$ and particles are point-like with $R = 0$.

The figures below present the results of calculations of the angular dependences of backscattering with just the coherent contribution taken into account at different degrees of anisotropy of the single scattering indicatrix. Specifically, Figs. 2 and 3 show the angular dependences of the CBS peak calculated for the HG and RG phase functions, respectively. Calculations with the RG phase function applied to a system of point particles characterize the results of isotropic scattering. A comparison of these calculations with the results obtained with the HG phase function at $g = 0$ reveals that they are virtually matching with satisfactory accuracy. However, as the scattering anisotropy grows, the angular dependences start to differ noticeably, and the discrepancy becomes significant when the scatterer size comes close to the wavelength. While the CBS peak remains quite narrow in calculations performed with the HG phase function, calculations based on the RG model reveal a significant broadening of the peak, which indicates that CBS may be used in biomedical applications.

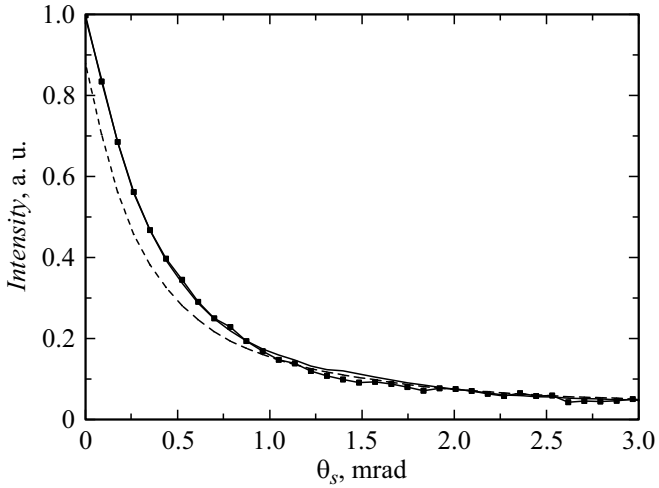

Figure 2. Dependence of the CBS intensity on angle θ_s in the HG model for media with a given anisotropy parameter: dashed curve — $g = 0.001$, solid curve — $g = 0.772$, and curve with filled squares — $g = 0.925$.

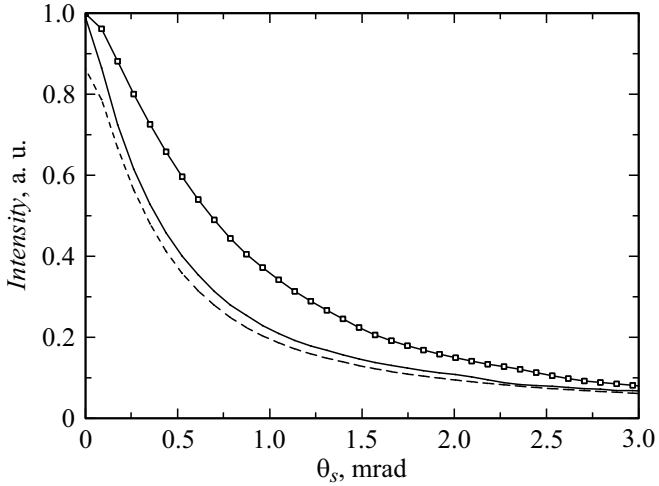

Figure 3. Dependence of the CBS intensity on angle θ_s in the RG model for media with a given scatterer radius: dashed curve — $R = 0.001\,\mathrm{nm}$, solid curve — $R = 250\,\mathrm{nm}$, and curve with filled squares — $R = 500\,\mathrm{nm}$.

The dependence of results on technical parameters of calculations (in particular, the choice of joining points for the intervals of approximation of the integral distribution function in the RG model) grows stronger as the phase function anisotropy increases. The CBS peak broadening is observed in all cases, but the quantitative description is unstable. According to [36,37], the observed broadening of the CBS peak is attributable to a reduction in the coherence of incident radiation, and this broadening is accompanied by a significant reduction in height of the peak itself. The peak height in these studies was about 8% of the theoretically predicted height calculated from the

incoherent ladder contribution. To characterize the effect of a reduction in spatial coherence of incident radiation on CBS, we performed calculations with restrictions on total number of scatterings n_{sc}. It was assumed that n_{sc} may be regarded as the number of scatterings after which the phase of oscillations loses consistency and becomes random. Spatial coherence length L_c was taken equal to $L_c = n_{sc} l_s$. Having denoted the backscattering intensity calculated from ladder diagrams only starting from double scattering (i.e., the main incoherent part) as $J_L(\theta_s)$ and the coherent component calculated based on maximally crossed diagrams as $J_C(\theta_s)$, we define the CBS enhancement parameter as $h(0) = (J_L(0) + J_C(0))/J_L(0)$.

The values of CBS enhancement parameter $h(0)$ determined in almost all experimental studies (even pioneering ones [12,14,38]) are noticeably lower than the maximum theoretical value of $h(0) = 2$. Specifically, experimental value $h(0) = 1.64$, which matches the result of our numerical calculations at $n_{sc} = 340$, was obtained in [12]. CBS peak half-width $\theta_{HW} = 1.50$ mrad calculated at this n_{sc} also agrees well with the experimental value of $\theta_{HW} = 1.58$ mrad [12].

Figures 4 and 5 present the angular dependences of CBS in half-spaces with media in which the scattering anisotropy is modeled by the HG and RG phase functions, respectively. In calculations with the HG indicatrix, the anisotropy parameter was taken equal to $g = 0.925$; the RG indicatrix was taken for particles with radius $R = 500$ nm, which corresponds to the same anisotropy parameter value. These figures show how the angular dependences of CBS (primarily the height and half-width of the peak) change with a reduction in the number of scatterings taken into account (n_{sc}) and, consequently, spatial coherence length $L_c = l_s n_{sc}$. The overall result of modeling with both phase functions is that the peak loses its height (with a simultaneous increase in its FWHM) as the coherence length decreases. It is also evident that the peaks calculated using the RG model are broader and almost always higher than the ones obtained with the HG phase function at the same L_c values.

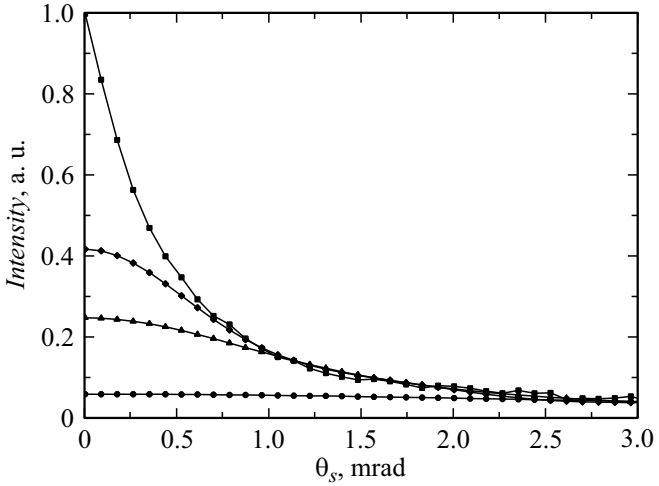

Figure 4. Dependence of the CBS intensity on angle θ_s in the HG model for media with a given number of scatterings. Squares — $n_{sc} = 5000$, diamonds — $n_{sc} = 100$, triangles — $n_{sc} = 50$, and circles — $n_{sc} = 15$.

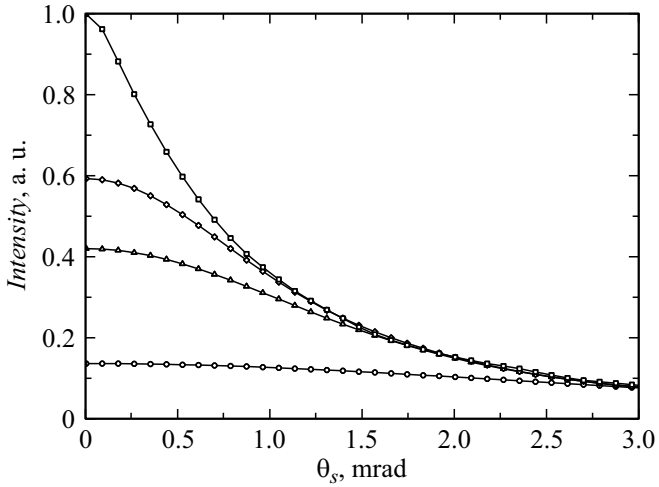

Figure 5. Dependence of the CBS intensity on angle θ_s in the RG model for media with a given number of scatterings. Squares — $n_{sc} = 5000$, diamonds — $n_{sc} = 100$, triangles — $n_{sc} = 50$, and circles — $n_{sc} = 15$.

It is worth noting that the CBS effect for low-coherence optical radiation was used in [37] to study human colon tissue cancer. The $h(0)$ peak height determined in these experiments was close to 1.07, and the half-width was $\theta_{HW} \approx 3.5$ mrad. Our MC modeling yields the same $h(0)$ value at $n_{sc} = 20$.

6. Conclusion

Comparative modeling of the CBS effect with anisotropy characterized using the HG and RG phase functions was performed based on the Bethe–Salpeter equation for transfer of optical radiation in a randomly inhomogeneous medium. An analytical inverse transform method for the angular integral distribution function has been implemented for the first time in the MC algorithm for the RG indicatrix. A piecewise smooth approximation was proposed for this distribution function. The results of calculations revealed that the RG model yields a broader and higher CBS peak than the HG model with the same degree of anisotropy of the single scattering indicatrix. Broadening of the CBS peak with a reduction in coherence of incident radiation was modeled. It turned out that this broadening in calculations performed with the RG phase function is more significant than the one in calculations with the HG indicatrix. The predicted broadening indicates that this effect has potential for application in biomedicine.

Funding

This study was supported by grant No. 23-22-00035 from the Russian Science Foundation, https://rscf.ru/project/23-22-00035/.

Conflict of interest

The authors declare that they have no conflict of interest.

References

[1] D.A. Boas, L.E. Campbell, A.G. Yodh. Phys. Rev. Lett., **75**, 1855 (1995). DOI: 10.1103/PhysRevLett.75.1855
[2] V.V. Tuchin. *Optika biologicheskikh tkanei. Metody rasseyaniya sveta v meditsinskoi diagnostike* (IPR Media, M., 2021) (in Russian).
[3] S.L. Jacques. Phys. Med. Biol., **58**, R37 (2013). DOI: 10.1088/0031-9155/58/11/R37
[4] D.J. Davies, Z. Su, M.T. Clancy, S.J. Lucas, H. Dehghani, A. Logan, A. Belli. J. Neurotrauma, **32**, 933 (2015). DOI: 10.1089/neu.2014.3748
[5] A. Sabeeh, V.V. Tuchin. J. Biomed. Photonics & Engineering, **6**, 040201 (2020). DOI: 10.18287/JBPE20.06.040201
[6] A.P. Tran, S. Yan, Q. Fang. Neurophoton, **7**, 015008 (2020). DOI: 10.1117/1.NPh.7.1.015008
[7] K. M. Watson. J. Math. Phys., **10**, 688 (1969). DOI: 10.1063/1.1664895
[8] D.A. de Wolf. IEEE Trans on Antennas and Propagation, **19**, 254 (1971). DOI: 10.1109/TAP.1971.1139894
[9] Yu.N. Barabanenkov. Radiophys. Quantum Electron., **16**, 65 (1973).
[10] A.G. Vinogradov, Yu.A. Kravtsov, V.I. Tatarskii. Radiophys. Quantum Electron., **16**, 818 (1973).
[11] Y. Kuga, A. Ishimaru. J. Opt. Soc. Am. A, **1**, 831 (1984).
[12] M. P. Van Albada, A. Lagendijk. Phys. Rev. Lett., **55**, 2692 (1985). DOI: 10.1103/PhysRevLett.55.2692
[13] P.-E. Wolf, G. Maret. Rev. Lett., **55**, 2696 (1985).
[14] E. Akkermans, P. Wolf, R. Maynard, G. Maret. J. Phys. France, **49**, 77 (1988). DOI: 10.1051/jphys:0198800490107700
[15] D.J. Pine, D.A. Weitz, P.M. Chaikin, E. Herbolzheimer. Phys. Rev. Lett., **60**, 1134 (1988).
[16] P. Wolf, G. Maret, E. Akkermans, R. Maynard. J. Phys. France, **49**, 63 (1988). DOI: 10.1103/PhysRevLett.60.1134
[17] F. Scholkmann, S. Kleiser, A.J. Metz, R. Zimmermann, J. Mata Pavia, U. Wolf, M. Wolf. Neuroimage, **85**, 6 (2014). DOI: 10.1016/j.neuroimage.2013.05.004
[18] H. Liu, D.A. Boas, Y. Zhang, A.G. Yodh, B. Chance. Phys. Med. Biol., **40**, 1983 (1995). DOI: 10.1088/0031-9155/40/11/015
[19] O. Pucci, V. Toronov, K. St Lawrence. Appl. Opt., **49**, 6324 (2010). DOI: 10.1364/AO.49.006324
[20] V.L. Kuzmin, Yu.A. Zhavoronkov, S.V. Ul'yanov, A.Yu. Valkov. J. Exp. Theor. Phys., **134**, 661 (2022). DOI: 10.31857/S0044451022060013
[21] J. Zhao, H.S. Ding, X.L. Hou, C.L. Zhou, B. Chance. J. Biomed. Opt., **10**, 024028 (2005). DOI: 10.1117/1.1891345
[22] V. Ntziachristos, B. Chance. Med. Phys., **28**, 1115 (2001). DOI: 10.1118/1.1373674
[23] A. Torricelli, D. Contini, A. Pifferi, M. Caffini, R. Re, L. Zucchelli, L. Spinelli. Neuroimage, **85**, 28 (2014). DOI: 10.1016/j.neuroimage.2013.05.106
[24] H. Wabnitz, J. Rodriguez, I. Yaroslavsky, A. Yaroslavsky, V. V. Tuchin. *Handbook of Optical Biomedical Diagnostics. Light-Tissue Interaction,* 2nd ed., Vol. 1 (SPIE Press, Bellingham, Washington, 2016).
[25] T. Durduran, R. Choe, J.P. Culver, L. Zubkov, M.J. Holboke, J. Giammarco, B. Chance, A.G. Yodh. Phys. Med. Biol., **47**, 2847 (2002). DOI: 10.1088/0031-9155/47/16/302
[26] M.A. Franceschini, S. Thaker, G. Themelis, K.K. Krishnamoorthy, H. Bortfeld, S.G. Diamond, D.A. Boas, K. Arvin, P.E. Grant. Frequency-Domain Near-Infrared Spectroscopy, Pediatr. Res., **61**, 546 (2007). DOI: 10.1203/pdr.0b013e318045be99
[27] A. Ishimaru. *Wave Propagation and Scattering in Random Media.* DOI: 10.1016/B978-0-12-374701-3.X5001-7
[28] V.L. Kuz'min, A.Yu. Val'kov, L.A. Zubkov. J. Exp. Theor. Phys., **128**, 396 (2019). DOI: 10.1134/S1063776119020109
[29] I.M. Sobol'. *Chislennye metody Monte-Karlo* (Nauka, M., 1973) (in Russian).
[30] V.L. Kuzmin, V.P. Romanov, E.V. Aksenova. Phys. Rev. E, **65**, 016601 (2001). DOI: 10.1103/PhysRevE.65.016601
[31] T.M. Nieuwenhuizen J. M. Luck. Phys. Rev. E, **48**, 569 (1993).
[32] L. Wang, S. L. Jacques, L. Q. Zheng. Comput. Meth. Prog. Bio., **47**, 131 (1995). DOI: 10.1016/0169-2607(95)01640-F
[33] L. Devroye. *Non-Uniform Random Variate Generation* (Springer, New York, 1986).
[34] V.L. Kuzmin, A.Yu. Val'kov. JETP Lett., **105**, 283 (2017). DOI: 10.1134/S0021364017050101
[35] S. Chandrasekhar. *Radiative Transfer* (Clarendon Press, 1950).
[36] Y.L. Kim, P. Pradhan, H. Subramanian, Y. Liu, M.H. Kim, V. Backman. Opt. Lett., **31**, 1459 (2006). DOI: 10.1364/OL.31.001459
[37] Y. L. Kim, Y. Liu, V.M. Turzhitsky, H.K. Roy., R.K. Wali, H. Subramanian, P. Pradhan, V. Backman. J. Biomed. Opt., **11**, 041125 (2006). DOI: 10.1117/1.2236292
[38] D.S. Wiersma, M.P. van Albada, A. Lagendijk. Phys. Rev. Lett., **75**, 1739 (1995). DOI: 10.1103/PhysRevLett.75.1739

Translated by D.Safin